An Efficient Biocatalytic System for Biosensing by Combining Metal-Organic Framework (MOF)-based Nanozymes and G-quadruplex (G4)-DNAzymes

Xuanxiang Mao, Fangni He, Dehui Qiu, Shijiong Wei, Rengan Luo, Yun Chen, Xiaobo Zhang, Jianping Lei, David Monchaud, Jean-Louis Mergny, et al.

An Efficient Biocatalytic System for Biosensing by Combining Metal-Organic Framework (MOF)-based Nanozymes and G-quadruplex (G4)-DNAzymes

Xuanxiang Mao,[1] Fangni He,[1] Dehui Qiu,[1] Shijiong Wei,[1] Rengan Luo,[1] Yun Chen,[1] Xiaobo Zhang,[1] Jianping Lei,[1] David Monchaud,[2] Jean-Louis Mergny,[1,3] Huangxian Ju,[1] Jun Zhou[1*]

[1]State Key Laboratory of Analytical Chemistry for Life Science, School of Chemistry and Chemical Engineering, Nanjing University, Nanjing 210023, PR China.

[2]Institut de Chimie Moléculaire (ICMUB), CNRS UMR6302, UBFC Dijon, 21078, France.

[3]Laboratoire d'Optique et Biosciences, Ecole Polytechnique, CNRS, INSERM, Institut Polytechnique de Paris, 91128 Palaiseau cedex, France.

ABSTRACT: A high catalytic efficiency associated to a robust chemical structure are among the ultimate goals when developing new biocatalytic systems for biosensing applications. To get ever closer to these goals, we report here on a combination of metal-organic framework (MOF)-based nanozymes and G-quadruplex (G4)-based catalytic system known as G4-DNAzyme. This approach aims at combining the advantages of both partners (chiefly, the robustness of the former, the modularity of the latter). To this end, we used MIL-53(Fe) MOF and linked it covalently to a G4-forming sequence (F3TC), itself covalently linked to its cofactor hemin. The resulting complex (referred to as MIL-53(Fe)/G4-hemin) exhibited exquisite peroxidase-mimicking oxidation activity and an excellent robustness (being stored in water for weeks). These properties were exploited to devise a new biosensing system, based on a cascade of reactions catalyzed by the nanozyme (ABTS oxidation) and an enzyme, the alkaline phosphatase (or ALP, ascorbic acid 2-phosphate dephosphorylation). The product of the latter poisoning the former, we thus designed a biosensor for ALP (a marker of bone diseases and cancers), with a very low limit of detection (LOD, 0.02 U L^{-1}) which is operative in human plasma samples.

Nanozymes are defined as nanomaterials with enzyme-mimicking activities. They have recently attracted a great deal of interest for their applications in bioanalysis, disease diagnosis,[1] and therapy. [1,2] Compared with natural proteinaceous enzymes, nanozymes display exceptional properties (e.g., chemical stability), versatility (e.g., easy chemical modifications)[2,3] and affordability. Since the pioneering report by Yan et al. about the peroxidase-like activity of ferromagnetic nanoparticles (Fe_3O_4 MNPs),[4] many other nanomaterials were studied including complexes made of noble metals[5,6] and metal oxides,[7,8] along with metal-organic frameworks (MOFs)[9,10] and derivatives.[11,12]

Among them, MOFs are of particular interest since these crystalline porous materials display appealing properties in terms of dimensions, surface-to-volume ratio, and well-defined and controllable chemical structure.[13] This was demonstrated for instance with MOFs made of NH_2-MIL-88(Fe),[14] MIL-53(Fe)[15] and 2D Fe-BTC nanosheets.[16] When used as nanozymes for peroxidase-type catalysis, MOF nanoparticles (NPs) have two major drawbacks:[17,18] a low catalytic activity, due to the limited active site exposure to the substrate,[17] and a weak colloidal stability, due to the aggregation/precipitation of MOF NPs in aqueous solutions.[18]

Herein, we report on our efforts to improve the catalytic properties of MOF NP nanozymes. To this end, we will exploit the biocatalytic properties of G-quadruplex-DNA (G4-DNA), known as G4-DNAzyme, and combine them with the MOF NP architectures. The catalytic properties of G4-DNAzyme relies on the interaction of the natural enzyme cofactor Fe(III)-protoporphyrin IX (hemin) with a four-strand higher DNA structure, a G4. This catalytic system, initialed uncovered by Sen et al.,[19] is particularly efficient for the oxidation of chromogenic substrates such as 3,3',5,5'-tetramethylbenzidine (TMB), 2,2'-azino-bis(3-ethylbenzothiazoline-6-sulfonic acid) (ABTS) and luminol, in the presence of H_2O_2. Their oxidation provides remarkable and easily monitorable color variations, making them useful for biosensing applications applied to the detection of proteins,[20,21] DNA strands,[22] small molecules (e.g., ATP),[23,24] and metal ions.[25,26] As above, this system is not devoid of drawbacks, chiefly a low catalytic activity when compared to the natural horseradish peroxidase (HRP).[27-30]

A strategy to improve G4-DNAzyme properties is to covalently link the G4 to its cofactor hemin. This complex, hereafter referred to as G4-hemin, is a far more efficient biocatalytic system.[31] Thus, we decided to combine the properties of G4-hemin with that of aforementioned MOF NPs, in order to study the catalytic activity of an original MOF/G4-hemin system, and compare its properties with a similar assembly in which the hemin is not covalently bound (MOF/G4/hemin).[24]

The series of results reported here unambiguously demonstrates the better performances of the MOF/G4-hemin nanozymatic system. As a proof-of-concept, we synthesized the iron (III) benzene dicarboxylate MOF known as MIL-53(Fe) (for Matériaux de l'Institut Lavoisier), initially developed by Férey et al.,[32] and linked it to G4-hemin complexes. The resulting MIL-53(Fe)/G4-hemin NPs display exquisite peroxidase-mimicking activity. This system was then used as a biosensor for the detection of the alkaline phosphatase (ALP): this enzyme, which catalyzes the dephosphorylation of

proteins and nucleic acids, is found in mammalian fluids and tissues. Its value for diagnostic purposes is firmly established because it is abnormally expressed notably in bone diseases (osteosarcomas, Paget's diseases) and cancers (e.g., liver cancer).[33] Here we used MIL-53(Fe)/G4-hemin NPs for detecting ALP according to a catalytic cascade that lead to the very sensitive detection (0.02 U L^{-1}) of this enzyme in human serum samples.

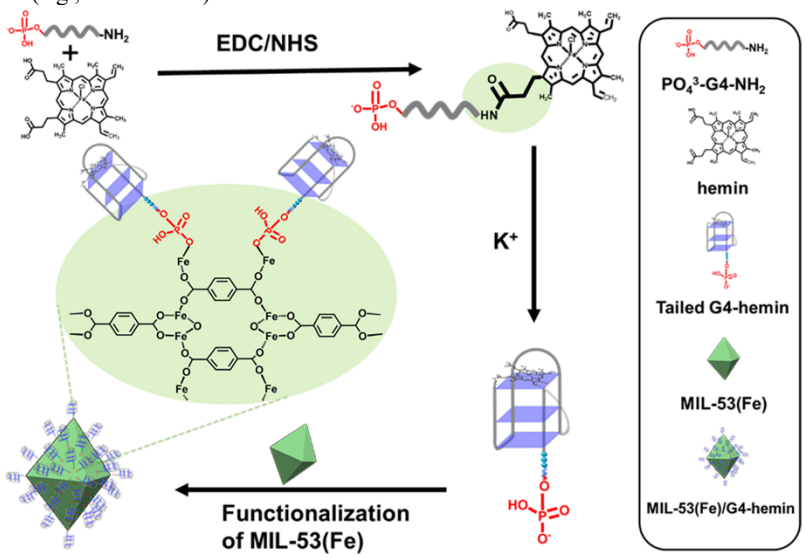

Scheme 1. Schematic representation of tailed phosphate modified G-quadruplex-hemin functionalized MIL-53(Fe) MOF nanoparticles. Hemin was first conjugated to the 3' end of PO_4^{3-}-G4-NH_2 and formed covalently linked tailed phosphate-modified G4-hemin, then conjugated to the surface of MIL-53(Fe) by straightforward metal-phosphate coordination to form MIL-53(Fe)/G4-hemin NPs.

EXPERIMENTAL SECTION

Synthesis of MIL-53(Fe) MOF. MIL-53(Fe) was synthesized according to a previously reported method[34] with slight modifications. Typically, 1.35 g $FeCl_3 \cdot 6H_2O$, 0.83 g 1,4-benzenedicarboxylic acid (BDC) and 25 mL N,N-dimethylformamide (DMF) were mixed and vigorously stirred for 30 min. Then, the mixture was poured into a 100 mL Teflon-lined steel autoclave and heated in an oven at 150 °C for 6 h. The obtained products were gathered by centrifugation (7000 rpm, 6 min), washed three times with ethanol and deionized water and dried at 60 °C in a vacuum for 12 h. Next, the obtained powder was suspended in ethanol, followed by stirring for 24 h. Finally, the powder was dried in a vacuum oven at 120 °C for 12 h to entirely remove solvent molecules within the frameworks of MIL-53(Fe) NPs and obtain coordination unsaturated Fe sites.

Preparation of covalent G4-hemin. The preparation method of covalent G4-hemin was as follows: 1 mL hemin DMSO solution (5 mM) was reacted with 0.5 mL of EDC and NHS solution (5 mM each) with stirring for 2 h at ambient temperature to activate the carboxyl group of hemin. Then, 10 μM DNA-NH_2, amine modified DNA sequences, dissolved in 10 mM Tris-HCl (pH 7.0) buffer was reacted with 40 μM activated NHS-hemin and 0.1 mg mL^{-1} 4-dimethylaminopyridine, and the resultant solution was reacted at 4 °C overnight. The resulting samples were heated to 95 °C for 5 min, cooled slowly to room temperature and stored at 4 °C prior to use.

Covalent linking of G4-hemin to MIL-53(Fe). The synthesis method of MIL-53(Fe)/G4-hemin is as follows: 1 mL 1.4 mg mL^{-1} MIL-53(Fe) MOFs was dispersed into 1 mL 2 μM G4-hemin solution, and stirred at room temperature for 12 h. Subsequently, the products were gathered after washing and centrifuging at 7000 rpm for 6 min, and dispersed in water with 100 mM KCl for following experiments.

Peroxidase mimetic-like activity evaluation. Peroxidase-mimicking activities of MIL-53(Fe)/G4-hemin NPs were estimated by monitoring the absorbance variation at 420 nm using the substrate ABTS. Typically, 50 μg mL^{-1} MIL-53(Fe)/G4-hemin were added to the mixture of 10 mM B-R buffer (pH 6.0) with 100 mM KCl, 0.1 mM H_2O_2 and 0.1 mM ABTS. Control experiments of MIL-53(Fe)/G4 NPs and G4-hemin were conducted similarly. The mixed solution was incubated at 37 °C, the absorbance of mixed solution at 420 nm (A_{420}) was recorded on a Cary 3500 UV-vis spectrophotometer (Agilent Technologies, CA, USA).

Colorimetric assay of alkaline phosphatase (ALP). ALP activity detection was performed as follows: 0.2 mM 2-phosphate trisodium salt (AAP), 25 μL of ALP with different activities ranging from 0 to 2000 U L^{-1} and 50 μL of Tris-HCl (10 mM, pH 8.0) were first mixed, and incubated at 37 °C for 30 min. Then, 330 μL B-R buffer (10 mM, pH 6.0) was added. Subsequently, 20 μg mL^{-1} MIL-53(Fe)/G4-hemin, 0.1 mM ABTS and 0.1 mM H_2O_2 were mixed, and the A_{420} was recorded after incubation at 37 °C for another 10 min. To detect ALP activity in real clinical samples, human serum samples (from Jiangsu Province Hospital, Nanjing) were treated via ultrafiltration with 30 kDa Amicon cell at 3000 rpm for 30 min, and the filtrate was employed for ALP analysis. All measurements were repeated three times.

RESULTS AND DISCUSSION

As shown in Scheme 1, the MIL-53(Fe)/G4-hemin catalysts were synthesized through a metal-phosphate coordination strategy, functionalizing the MOF NPs with a phosphate-modified G4-hemin. To this end, hemin was first covalently conjugated to the 3'-end of PO_4^{3-}-G4-NH_2 via an EDC/NHS strategy, the G4 structures annealed via a thermal treatment in a K^+-rich buffer (the sequences are provided in Table S1), and the final complex assembled by mixing the MIL-53(Fe) MOF with G4-hemin for 12 h at room temperature. Of note, it was previously demonstrated that the coordination of the terminal phosphate group with the metal ions of the MOFs is favored over an interaction through the DNA backbone's phosphate groups, for steric hindrance reasons.[35]

The efficiency of this experimental setup was demonstrated with the synthesis of a series of MOFs based on different metal ions and ligands (HKUST-1, PCN-224, PCN-222, UIO-66, ZIF-8/67/90,

Zn-hemin MOF, MIL-53/88B/101, see the Supporting Information) conjugated with our model G4-hemin, F3TC-hemin.[36] The catalytic activity of the resulting MOF/G4-hemin NPs was evaluated with the H_2O_2-mediated oxidation of ABTS[37] (Figure 1A): the strongest improvement as compared to both the MOF alone and F3TC-hemin was obtained with the MIL-53(Fe)/G4-hemin nanozyme, evidenced by the maximum absorbance, thus selected for subsequent investigations.

We thus decided to gain more information about the actual structure of MIL-53(Fe)/G4-hemin, using a combination of physical and physicochemical methods. As shown in Figure 1B, the X-ray diffraction (XRD) patterns of the prepared MIL-53(Fe) fully matches the simulated MIL-53(Fe)[38] with, however, a slight decrease in intensities of the characteristic peaks, suggesting at small decomposition after heating at 120 °C for 12 h, revealed by several coordinated unsaturated (CUS) Fe atoms in MIL-53(Fe).[34,39] Importantly, the XRD signature was not affected by the conjugation of G4-hemin, demonstrating that the overall structure of the MOF was preserved. The generality of this observation was assessed by the analysis of the XRD patters of the MOF NPs built from HKUST-1, PCN-224, UIO-66, ZIF-8/67/90 and MIL-88B/101, PCN-222, Zn-hemin MOF (see Figure S1). We also analyzed the scanning electron microscopy (SEM) images of both MIL-53(Fe) and MIL-53(Fe)/G4-hemin (Figures 1C and S2A). Both MOFs display octahedral shapes, confirming again that the conjugation of G4-hemin does not affect its overall structure. After functionalization of G4-hemin into the MIL-53(Fe), as characterized by dynamic light scattering (DLS), the size of MIL-53(Fe)/G4-hemin was slightly larger than that of bare MIL-53(Fe), demonstrating the combination of G4-hemin with MOF (Figures S2B and S2C).

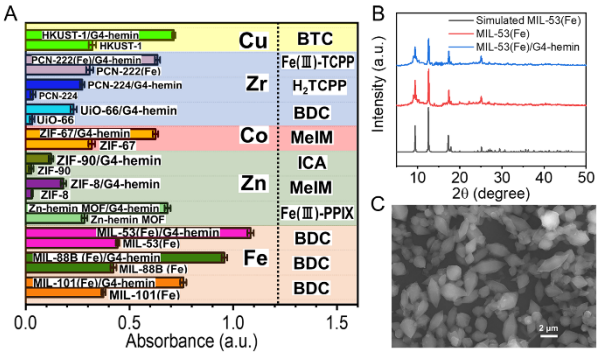

Figure 1. (A) Effects of different MOFs on catalytic activity with F3TC-hemin (different MOFs contains a series of metal nodes and ligands. Metal nodes includes Cu, Zr, Co, Zn, Fe, ligands includes trimesic acid (BTC), tetrakis(4-carboxyphenyl)porphyrin (H_2TCPP), 1,4-benzenedicarboxylic acid (BDC), 2-methylimidazole (MeIM), imidazole-2-carboxaldehyde (ICA), [5,10,15,20-tetrakis(4-methoxycarbonylphenyl)porphyrinato]-Fe(III) chloride (Fe(III)-TCPP), Fe(III)-protoporphyrin IX (Fe(III)-PPIX), the concentrations of catalysts were 30 mg L^{-1}; (B) Power X-ray diffraction patterns of simulated MIL-53(Fe), obtained MIL-53(Fe) samples and MIL-53(Fe)/G4-hemin; and (C) SEM images of MIL-53(Fe) covalently linker with G4-hemin.

Next, we sought to demonstrate the presence of the G4 onto the surface of the MOF. To this end, the Fourier-transform infrared (FT-IR) spectra of G4-hemin, MIL-53(Fe) and MIL-53(Fe)/G4-hemin were collected and compared. As seen in Figure S3, the spectra of MIL-53(Fe)-containing species comprised numerous peaks typical of the C-H bending vibrations of the benzene rings (749 cm^{-1}) and of the Fe-O bonds (538 cm^{-1}) within the MOF, confirming the Fe/terephthalic acid nodes.[40] Importantly, the spectra of the G4-hemin-contianing species comprised a peak at 1046 cm^{-1} that is characteristic of the G4-hemin complex, thus demonstrating that the MIL-53(Fe)/G4-hemin was successfully constructed. This was further investigated by the thermogravimetric analysis of both MIL-53(Fe) and MIL-53(Fe)/G4-hemin (Figure S4). It was indeed found that the conjugation of the G4-hemin indeed provided a better thermal stability to the edifice, therefore indicating that structure of the NPs was indeed modified (and that the resulting conjugate displayed excellent thermal stability).

To verify the generation of iron CUS during vacuum heating and analyze the chemical states of the P, O and Fe elements, X-ray photoelectron spectroscopy (XPS) was also used. This analysis of MIL-53(Fe) confirmed that only C, Fe and O elements were present (Figure 2A), while no N elements were detectable, indicating that the solvent N, N-dimethylformamide (DMF) molecules, coordinated to the Fe atoms of the MOF, were successfully removed during the heating step, thus indicating the presence of iron CUS.[34] In contrast, the XPS analysis of MIL-53(Fe)/G4-hemin showed the presence of C, Fe, O, N and P elements, indicating again that G4-hemin was indeed connected on the surface of the MOF.

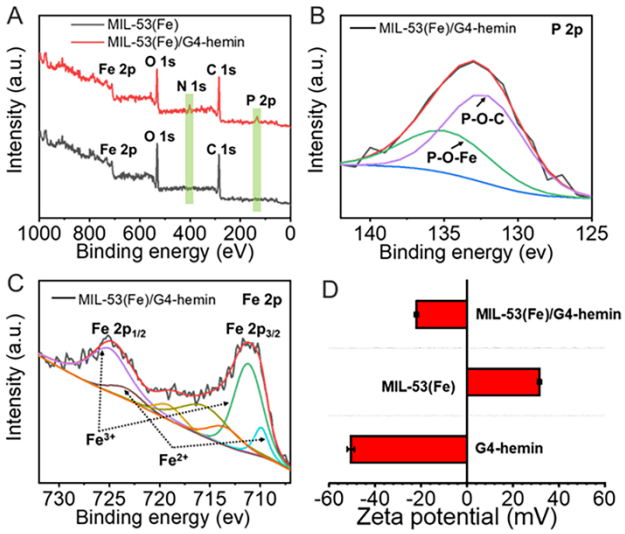

Figure 2. (A) XPS survey spectra of MIL-53(Fe) before and after modification with G4-hemin. (B and C) XPS spectra of MIL-53(Fe)/G4-hemin: (B) P 2p, (C) Fe 2p. (D) Zeta potentials of G4-hemin, MIL-53(Fe) and MIL-53(Fe)/G4-hemin.

The analysis of the P 2p spectrum of MIL-53(Fe)/G4-hemin provided a direct evidence of the nature of the link between the MOF and the G4 since a peak at 135.8 eV, which is characteristic of the formation of P-O-Fe bonds,[41] is clearly seen in Figure 2B. We also analyzed the Fe 2p spectrum (Figure 2C), which provides typical signature of Fe^{3+} (711.2 eV, 719.0 eV and 725.0 eV) and Fe^{2+} (709.9 eV, 715.5 eV and 723.4 eV),[34,42] and the O 1s spectrum of MIL-53(Fe)/G4-hemin (Figure S5), which further confirmed the presence of a O-Fe bound (at 530.2 eV), along with typical P=O, P-OH and O-C=O bonds (at 531.5 eV, 531.8 eV and 532.7 eV, respectively).[42]

We finally measured the ζ potential of MIL-53(Fe), G4-hemin and MIL-53(Fe)/G4-hemin. The results seen in Figure 2D again advocate for the formation of a covalent MOF-G4 complex as the ζ potential significantly decreased from +31.5 to -22.1 mV after G4-hemin conjugation.

Another way to gain further insights into the covalent connection between MIL-53(Fe) and G4-hemin was to fluorescently label the G4 (adding a 6-carboxyfluorescein (FAM) at its 3'-end) and perform fluorescence investigations. The confocal pattern diagrams seen in Figures S6A-C showed that when FAM-labeled G4s were

covalently linked to MIL-53(Fe) NPs, a bright fluorescence response can be observed at 527 nm, perfectly overlapping the NPs (bright field). We next performed energy dispersive spectroscopy (EDS) elemental mapping, which confirmed the O, N, P and Fe elements in the MIL-53(Fe)/G4-hemin (Figures S6D-I).

After these physical and physicochemical characterizations that provided a clear overview of the overall structure of MIL-53(Fe)/G4-hemin, we decided to further investigate its catalytic properties. We described above that the nature of the MOF has a significant impact on the catalytic properties of the resulting complexes. We thus investigated the nature of the G4-forming sequences, combined to MIL-53(Fe). As seen in Figure 3A, we built and compared MOF with 22 different G4 DNAs, not covalently linked to hemin. These investigations confirmed the relevance of our first choice, as F3TC display the best catalytic activity (with an initial velocity V_0 of 15.63 x 10^{-7} M s^{-1}). The result was consistent with our previous observations, the enhanced catalytic properties originating in the presence of the proximal nucleobases dC.[43] These results also further demonstrated the interest of covalently link the hemin to the 3' end of F3TC, as the conjugated system is *ca*. 1.5-fold more competent than the noncovalent F3TC/hemin complex. This result confirmed by a series of UV-Vis control experiments (Figure 3B). Interestingly, the synergy effect between MOF and G4 DNAzyme was observed for the first time, as the used MIL-53(Fe) MOF here possess higher HRP like activity than previous used.[44,45] As displayed in Figure 3B, both G4-hemin and MIL-53(Fe)/G4 can catalyze the oxidation of ABTS by H_2O_2. However, the catalytic activity of noncovalent G4/hemin modified on the surface of MIL-53(Fe) did not increase significantly. The potential reason is the weak π-π stacking between hemin and MIL-53(Fe)/G4 resulting in the dissociation of them easily. Moreover, the MIL-53(Fe)/G4-hemin significantly increased the peroxidase-like activity, demonstrating the synergistic effect of active sites between inner MIL-53(Fe) and outer covalent G4-hemin, which may be attributed to two points: The hydrophilic G4-hemin improves the dispersion of MIL-53(Fe) in water, and the scattered MIL-53(Fe) further prevents the dimerization of G4-hemin when it was covalently linked to the surface of MIL-53(Fe).

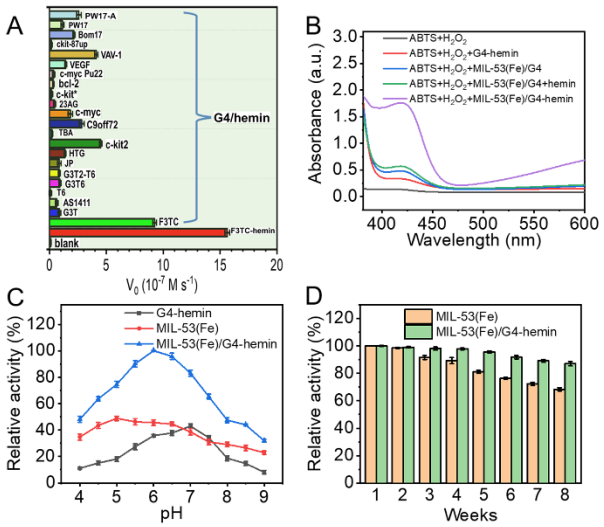

Figure 3. (A) Effects of various G4 DNA (1 µM) on catalytic activity, (B) UV-vis absorbance spectra of the ABTS-H_2O_2 system in the presence of G4-hemin (9 nM), MIL-53(Fe) (50 mg L^{-1}) and G4 (9 nM) in the absence or presence of free hemin, or covalent linked MIL-53(Fe) and G4-hemin (50 mg L^{-1}). (C) The pH effect of G4-hemin, MIL-53(Fe) and MIL-53(Fe)/G4-hemin over a range of pH between 4.0 to 9.0; (D) The stability of MIL-53(Fe)/G4-hemin as peroxidase mimic in aqueous solution. Error bars denote standard deviations based on three measurements.

Next, we investigated the various parameters that could influence the catalytic properties of MIL-53(Fe)/G4-hemin. Firstly, we varied the amount of MIL-53(Fe) with respect to that of G4-hemin: the optimal ratio was found to be 0.7 mg mL^{-1} of MIL-53(Fe) for 1 µM of G4-hemin (Figure S7). In these conditions, an atomic emission spectroscopy by inductive coupling plasma (ICP-AES) analysis indicated a coverage ratio of 9±1 nmol mg^{-1} DNA for MIL-53(Fe) NPs. Secondly, the pH and the temperature of the experiments along with the concentration of ABTS, catalyst and H_2O_2 were optimized. While the optimum pH for experiments performed with G4-hemin and MIL-53(Fe) was found to be 7.0 and 5.0, respectively, that of MIL-53(Fe)/G4-hemin was pH 6.0 (Figure 3C). The catalytic activity of this complex increased with the concentration of ABTS (0 to 200 µM) and H_2O_2 (0 to 800 µM) and MIL-53(Fe)/G4-hemin (0 to 100 mg L^{-1}, Figures S8A-C). This activity also raised with the temperature (25 to 60 °C, Figure S8D). Therefore, the experimental setups for subsequent investigations was fixed at 100 µM ABTS, 300 µM H_2O_2, 50 mg L^{-1} MIL-53(Fe)/G4-hemin at 37 °C and pH 6.0.

Interestingly, the presence of a linked G4 provided a protection against MOF deactivation, as *ca*. 37% of the initial activity of MIL-53(Fe) was lost after storing in aqueous solution for 8 weeks (certainly because of the aggregation of hydrophobic MOFs in water)[46] while only *ca*. 9% of the catalytic activity of MIL-53(Fe)/G4-hemin was lost in the same conditions (certainly due the improved water solubility of DNA-coated MOF along with the negative DNA charges that may promote dispersion of the NPs).

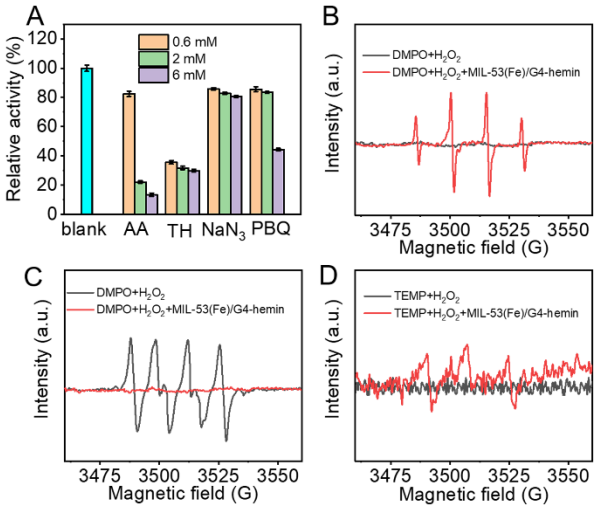

Figure 4. (A) Catalytic oxidation of ABTS in the presence of H_2O_2 and various radical scavengers. (B-D) The ESR spectra of the DMPO-H_2O_2-MIL-53(Fe)/G4-hemin in (B) aqueous suspension, (C) methanol solution, and (D) TEMP-H_2O_2-MIL-53(Fe)/G4-hemin in aqueous suspension.

We also looked at the mechanism of this novel nanozyme, which is still a matter of debate.[47] To this end, we used various radical scavengers such as ascorbic acid (AA) for •OH and $O_2^{\bullet-}$,[48] thiourea (TH) for •OH,[49] p-benzoquinone (p-BQ) for $O_2^{\bullet-}$[50] and NaN_3 for $^1O_2$.[51] The catalytic activity of MIL-53(Fe)/G4-hemin was strongly decreased upon addition of AA and TH, implying the generation of •OH and $O_2^{\bullet-}$ during the catalytic process (Figure 4A), which is fully in line with the most recent mechanism.[43] We performed electron spin resonance (ESR) experiments to confirm the production of •OH and $O_2^{\bullet-}$: as seen in Figure 4B, four characteristic peaks were clearly visible on the spectrum of MIL-53(Fe)/G4-hemin in water (1:2:2:1 ratio), confirming the production of •OH radicals. There peaks were also visible on the spectrum of MIL-53(Fe)/G4-

hemin in methanol (1:1:1:1 ratio), indicating generation of $O_2^{\bullet-}$ radicals (Figure 4C). The very weak signal obtained when using MIL-53(Fe)/G4-hemin with 2,2,6,6-tetramethyl-4-piperidine (TEMP) to trap $^1O_2$ in water confirmed that the production of $^1O_2$ is scarce in these conditions (Figure 4D).

We next decided to better characterize the kinetics of the reactions catalyzed by MIL-53(Fe)/G4-hemin. To this end, we varied the concentration of H_2O_2 (0 to 10 mM) in the presence of a fixed and high concentration of ABTS (0.06 mM) and *vice versa* (0 to 2 mM ABTS *versus* 0.02 mM H_2O_2). The Michaelis-Menten analyses of these reactions provided two parameters, the Michaelis-Menten constant (K_m) and the maximal reaction velocity (V_{max}). The curves seen in Figures 5A, B provided the parameters upon varying H_2O_2 concentrations, with K_m = 0.14 mM and V_{max} = 0.71×10^{-7} M s^{-1}. In the opposite setup, these values were 0.17 mM and 1.07×10^{-7} M s^{-1}, respectively (Table S2). The comparison of these values indicated a higher affinity of MIL-53(Fe)/G4-hemin for H_2O_2 and ABTS than other nanozymes, and even HRP.[52] We thus calculated the K_w value, which provides a measurement of the catalytic reaction rate,[53] and obtained a higher K_w value for MIL-53(Fe)/G4-hemin than for other nanozymes (Table S2). This exquisite efficiency was confirmed through the Lineweaver-Burk plots seen in Figures 5C, D: the observation of the lines were almost parallel with each other (and the slopes equal) conforming to a ping-pong mechanism that MIL-53(Fe)/G4-hemin reacted with the first substrate and released the first product before it interacted with the second one, in a manner that is analogous to HRP[52] and Fe_3O_4 nanoparticles.[4]

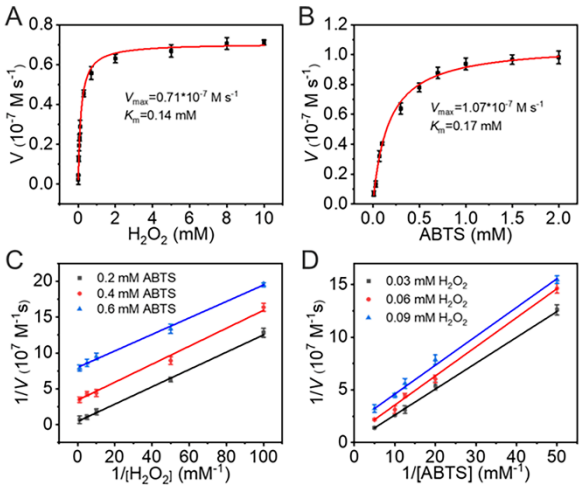

Figure 5. (A and B) Steady-state kinetic assay of MIL-53(Fe)/G4-hemin with (A) 0.06 mM ABTS and various concentration of H_2O_2, and (B) 0.02 mM H_2O_2 and various concentration of ABTS. (C and D) Double reciprocal plots of the activity of MIL-53(Fe)/G4-hemin with (C) fixed concentration of ABTS and varied concentration of H_2O_2, and (D) fixed concentration of H_2O_2 and various concentration of ABTS. Error bars denote standard deviations based on three measurements.

We demonstrated above that AA, an antioxidant and free radical scavenger, could hamper the oxidation of ABTS by H_2O_2.[54] Interestingly, orthophosphate monoester such as ascorbic acid 2-phosphate (AAP) could be hydrolyzed by the enzyme ALP to generate AA. This led us to devised a novel and simple colorimetric strategy for biosensing the activity of ALP based on our MIL-53(Fe)/G4-hemin system, in presence of ABTS and H_2O_2 (Figure 6A).

We thus checked the feasibility and reliability of this oxidation cascade, step by step. Firstly, we confirmed the inhibitory effect of AA (3 µM) on the activity of MIL-53(Fe)/G4-hemin (Figure 6B). Secondly, we verified the sensitivity of this inhibition by varying the concentration of MIL-53(Fe)/G4-hemin (0 to 100 µg mL^{-1}, Figure S9A) and ABTS (0 to 1 mM, Figure S9B), in the presence of 0 to 100 µM of AA: the inhibition was maximally felt for 20 µg mL^{-1} catalyst and 1 mM ABTS, which were thus selected for subsequent experiments. Further, the linear range of AA was 0.01-7 µM ($\Delta A = 0.0141 + 0.0636$ [AA], r^2 =0.9960, n = 12) with a limit of detection (LOD) of 0.01 µM according to 3δ/K, in which δ and K represent the standard deviation of blank samples (n=11) and slop of the liner regression equation, respectively (Figure 6C). Thirdly, we assessed the performances of ALP in these conditions (Figure 6D): the ABTS oxidation was inhibited only when both 20 U L^{-1} of ALP and 0.2 mM of AAP were mixed, due to the in situ generation of AA. Interestingly, the addition of p-bromotetramisole oxalate, an inhibitor of alkaline phosphatase, produce less AA, which make the ABTS oxidation effective in the presence of H_2O_2.

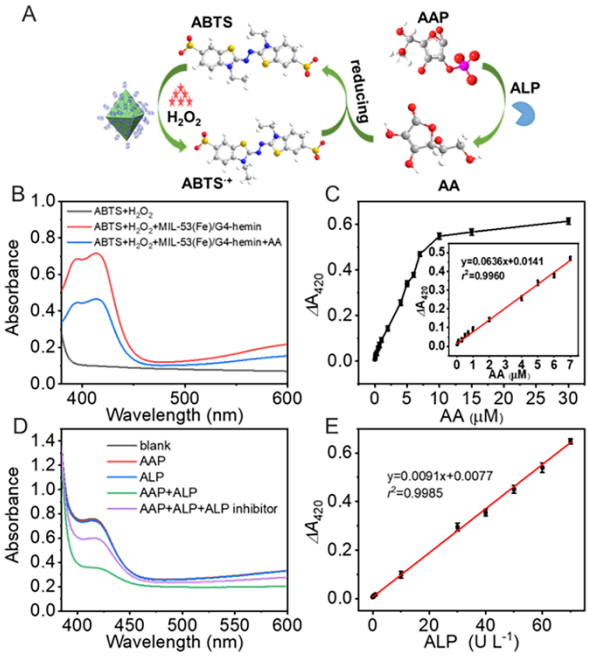

Figure 6. (A) Schematic illustration of sensing platform for ALP activity analysis. (B) The UV-vis absorption spectra of various reaction systems in the presence of 3 µM AA. (C) Linear plots of ΔA_{420} versus concentrations of AA (0-30 µM). Inset: The UV-vis absorption curves of MIL-53(Fe)/G4-hemin based colorimetric assay with different AA activities from 0.01-7 µM. (D) The UV-vis absorption spectra of various reaction systems in the presence of ALP. (E) Linear plots of ΔA_{420} versus concentrations of ALP (0.03-70 U L^{-1}).

It was thus of interest to lower the ALP concentration in order to define the limit of detection (LOD) of the biosensing system. The oxidation activity was directly linked, in a linear manner to the ALP concentration (0 to 70 U L^{-1}, Figures 6E and S9D), which corresponds to a broader range as compared to previously reported methods (Table S3). More importantly, this biosensor is found to be highly sensitive as the LOD is estimated at 0.02 U L^{-1} (3δ/K) (Table S3).

We next wondered whether, in addition to being sensitive, this system is specific. To this end, biomolecules usually found in human serum (proteins, amino acids, etc.) were used as potential triggers of this oxidation cascade: as depicted in Figure S10, huge excess (from 4- to 500-fold) did not affect the ALP/MIL-53(Fe)/G4-hemin reaction cascade (Figure S10). Then, the activity of this biosensing system was evaluated directly in human serum samples.

The ALP was added at 3 different concentration (0.4, 1 and 3 U L^{-1}) and the detection provided by the MIL-53(Fe)/G4-hemin-based system ranged between 92 to 101% (with a running slope difference (RSD) lower than 5.0% (Table 1)), which clearly highlighted not only the performances but also the reliability of our biosensor in real conditions.

Table 1. The determination result of ALP in real human serum samples

Serum Samples	Spiked (U L^{-1})	Found (U L^{-1})	Recovery (%)	RSD (%, n = 3)
1	0.4	0.37	92.50	3.56
	1	0.95	95.00	3.62
	3	3.04	101.33	2.43
2	0.4	0.38	95.00	3.98
	1	0.96	96.00	2.63
	3	2.87	95.67	3.74
3	0.4	0.39	97.50	3.85
	1	0.97	97.00	4.19
	3	2.93	97.67	3.66

CONCLUSIONS

In conclusion, the biocatalytic system reported here, MIL-53(Fe)/G4-hemin, combined the advantages of MOF-based nanozymes and G4-DNAzymes. Its synthesis is straightforward, *via* a facile metal-phosphate coordination strategy. Its excellent catalytic properties, along with a good chemical stability, makes it a highly valuable biosensor. This was demonstrated by sensitive detection of ALP activity, achieved through two intertwined catalytic cycles: the former relies on the ability of MIL-53(Fe)/G4-hemin to oxidize ABTS, which yield a series of radical species; the later relies on ALP, which dephosphorylates AAP to yield AA, a known scavenger of radicals. Therefore, the product of the latter poisons the former, which leads to a detection system that is not only sensitive, cost effective but also operative in real conditions. This work thus demonstrates that two efficient biosensors can be associated to act synergistically in order to provide an hybrid system that combines the benefits of the two methods.

ASSOCIATED CONTENT

Supporting Information

The Supporting Information is available free of charge on the ACS Publications website.

Introduction of chemicals, instrumentations, synthesis of eight MOF NPs, definition of the K_w value, electron spin resonance (ESR) experiment, sequences of G4 DNA oligonucleotides used in this work, comparison of the V_{max} and K_w values and kinetic parameters of MIL-53(Fe)/G4-hemin with other peroxidase mimetic-like activity, comparison of the current work with reported methods for the determination of ALP, power X-ray diffraction patterns of eleven MOF NPs, SEM images, DLS analysis, the FTIR spectra, thermogravimetric analysis curves, O 1s XPS spectra of MIL-53(Fe)/G4-hemin, confocal fluorescence micrographs, EDS elemental mappings, UV-vis absorption spectra, the Fluorescence emission spectrum, optimization of measurement conditions and selective experiment. (PDF)

AUTHOR INFORMATION

Corresponding Author

Jun Zhou - State Key Laboratory of Analytical Chemistry for Life Science, School of Chemistry and Chemical Engineering, Nanjing University, Nanjing 210023, PR China; orcid.org/0000-0002-6793-3169; Email: jun.zhou@nju.edu.cn

Authors

Xuanxiang Mao - State Key Laboratory of Analytical Chemistry for Life Science, School of Chemistry and Chemical Engineering, Nanjing University, Nanjing 210023, PR China; orcid.org/0000-0002-5843-7593; Email: DG1924064@smail.nju.edu.cn
Fangni He - State Key Laboratory of Analytical Chemistry for Life Science, School of Chemistry and Chemical Engineering, Nanjing University, Nanjing 210023, PR China; Email: mg20240030@smail.nju.edu.cn
Dehui Qiu - State Key Laboratory of Analytical Chemistry for Life Science, School of Chemistry and Chemical Engineering, Nanjing University, Nanjing 210023, PR China; orcid.org/0000-0002-0085-6832; Email: xhqdh@smail.nju.edu.cn
Shijiong Wei - State Key Laboratory of Analytical Chemistry for Life Science, School of Chemistry and Chemical Engineering, Nanjing University, Nanjing 210023, PR China; Email: weishijiong@smail.nju.edu.cn
Rengan Luo - State Key Laboratory of Analytical Chemistry for Life Science, School of Chemistry and Chemical Engineering, Nanjing University, Nanjing 210023, PR China; Email: DZ1824023@smail.nju.edu.cn
Yun Chen - State Key Laboratory of Analytical Chemistry for Life Science, School of Chemistry and Chemical Engineering, Nanjing University, Nanjing 210023, PR China; orcid.org/0000-0002-9295-0497; Email: chenyun@smail.nju.edu.cn
Xiaobo Zhang - State Key Laboratory of Analytical Chemistry for Life Science, School of Chemistry and Chemical Engineering, Nanjing University, Nanjing 210023, PR China; orcid.org/0000-0003-0222-2515; Email: xhzxb@nju.edu.cn
Jianping Lei - State Key Laboratory of Analytical Chemistry for Life Science, School of Chemistry and Chemical Engineering, Nanjing University, Nanjing 210023, PR China. Email: jpl@nju.edu.cn
David Monchaud - Institut de Chimie Moléculaire (ICMUB), CNRS UMR6302, UBFC Dijon, 21078, France. orcid.org/0000-0002-3056-9295; Email: david.monchaud@u-bourgogne.fr
Jean-Louis Mergny - State Key Laboratory of Analytical Chemistry for Life Science, School of Chemistry and Chemical Engineering, Nanjing University, Nanjing 210023, PR China; Laboratoire d'Optique et Biosciences, Ecole Polytechnique, CNRS, INSERM, Institut Polytechnique de Paris, 91128 Palaiseau cedex, France; orcid.org/0000-0003-3043-8401; Email: jean-louis.mergny@polytechnique.edu
Huangxian Ju - State Key Laboratory of Analytical Chemistry for Life Science, School of Chemistry and Chemical Engineering, Nanjing University, Nanjing 210023, PR China; orcid.org/0000-0002-6741-5302; Email: hxju@nju.edu.cn

Author Contributions

X.M. and J.Z. conceived and designed the study. X.M., F.H., D.Q., S.W., R.L. and Y.C. performed the experiments. X.M., F.H., D.Q., J.Z. and J.L. analyzed data. X.M. and J.Z. wrote the paper. X.M., X.Z., J.L., M.D., J.M., H.J., and J.Z. reviewed and edited the manuscript. All authors read and approved the manuscript.

ACKNOWLEDGMENT

The work has also been supported by the National Natural Science Foundation of China (21977045, 22177047, and 22004062), China Postdoctoral Science Foundation (2020M681543), and the funds of Nanjing University (020514912216).

REFERENCES

1. Wei, H.; Wang, E. Nanomaterials with enzyme-like characteristics (nanozymes): next-generation artificial enzymes. *Chem. Soc. Rev.* **2013**, *42*, 6060-6093.

2. Liang, M.; Yan, X. Nanozymes: From new concepts, mechanisms, and standards to applications. *Acc. Chem. Res.* **2019**, *52*, 2190-2200.

3. Wang, Q.; Wei, H.; Zhang, Z.; Wang, E.; Dong, S. Nanozyme: An emerging alternative to natural enzyme for biosensing and immunoassay. *TrAC, Trends Anal. Chem.* **2018**, *105*, 218-224.

4. Gao, L.; Zhuang, J.; Nie, L.; Zhang, J.; Zhang, Y.; Gu, N.; Wang, T.; Feng, J.; Yang, D.; Perrett, S.; Yan, X. Intrinsic peroxidase-like activity of ferromagnetic nanoparticles. *Nat. Nanotechnol.* **2007**, *2*, 577-583.

5. Tao, Y.; Ju, E.; Ren, J. S.; Qu, X. G. Bifunctionalized mesoporous silica-supported gold nanoparticles: intrinsic oxidase and peroxidase catalytic activities for antibacterial applications. *Adv. Mater.* **2015**, *27*, 1097-1104.

6. Jiang, X.; Wang, X.; Lin, A.; Wei, H. In situ exsolution of noble-metal nanoparticles on perovskites as enhanced peroxidase mimics for bioanalysis. *Anal. Chem.* **2021**, *93*, 5954-5962.

7. Wei., H.; Wang., E. Fe_3O_4 magnetic nanoparticles as peroxidase mimetics and their applications in H_2O_2 and glucose detection. *Anal. Chem.* **2008**, *80*, 2250-2254.

8. Jia, H.; Yang, D.; Han, X.; Cai, J.; Liu, H.; He, W. Peroxidase-like activity of the Co_3O_4 nanoparticles used for biodetection and evaluation of antioxidant behavior. *Nanoscale* **2016**, *8*, 5938-5945.

9. Huang, Y.; Zhao, M.; Han, S.; Lai, Z.; Yang, J.; Tan, C.; Ma, Q.; Lu, Q.; Chen, J.; Zhang, X.; Zhang, Z.; Li, B.; Chen, B.; Zong, Y.; Zhang, H. Growth of Au nanoparticles on 2D metalloporphyrinic metal-organic framework nanosheets used as biomimetic catalysts for cascade reactions. *Adv. Mater.* **2017**, *29*, 1700102-1700107.

10. Hu, W. C.; Pang, J.; Biswas, S.; Wang, K.; Wang, C.; Xia, X. H. Ultrasensitive Detection of Bacteria Using a 2D MOF Nanozyme-Amplified Electrochemical Detector. *Anal. Chem.* **2021**, *93*, 8544-8552.

11. Hou, Y.; Lu, Y.; Chen, Q.; Zhang, X.; Huang, Y. Ultrathin two-dimensional carbon nanosheets with highly active Cu-N_x sites as specific peroxidase mimic for determining total antioxidant capacity. *Sens. Actuators, B* **2021**, *333*, 129549-129558.

12. Li, J.; Xin, W. L.; Dai, Y. X.; Shu, G.; Zhang, X. J.; Marks, R. S.; Cosnier, S.; Shan, D. Postmodulation of the metal-organic framework precursor toward the vacancy-rich Cu_xO transducer for sensitivity boost: synthesis, catalysis, and H_2O_2 Sensing. *Anal. Chem.* **2021**, *93*, 11066-11071.

13. Niu, X.; Li, X.; Lyu, Z.; Pan, J.; Ding, S.; Ruan, X.; Zhu, W.; Du, D.; Lin, Y. Metal-organic framework based nanozymes: promising materials for biochemical analysis. *Chem. Commun.* **2020**, *56*, 11338-11353.

14. Liu, Y. L.; Zhao, X. J.; Yang, X. X.; Li, Y. F. A nanosized metal-organic framework of Fe-MIL-88NH_2 as a novel peroxidase mimic used for colorimetric detection of glucose. *Analyst* **2013**, *138*, 4526-4531.

15. Ai, L.; Li, L.; Zhang, C.; Fu, J.; Jiang, J. MIL-53(Fe): a metal-organic framework with intrinsic peroxidase-like catalytic activity for colorimetric biosensing. *Chem. Eur. J.* **2013**, *19*, 15105-15108.

16. Yuan, A.; Lu, Y.; Zhang, X.; Chen, Q.; Huang, Y. Two-dimensional iron MOF nanosheet as a highly efficient nanozyme for glucose biosensing. *J. Mater. Chem. B* **2020**, *8*, 9295-9303.

17. Lin, Y.; Ren, J.; Qu, X. Catalytically active nanomaterials: a promising candidate for artificial enzymes. *Acc. Chem. Res.* **2014**, *47*, 1097-1105.

18. Tan, H.; Ma, C.; Gao, L.; Li, Q.; Song, Y.; Xu, F.; Wang, T.; Wang, L. Metal-organic framework-derived copper nanoparticle@carbon nanocomposites as peroxidase mimics for colorimetric sensing of ascorbic acid. *Chem. Eur. J.* **2014**, *20*, 16377-16383.

19. Travascio, P.; Li, Y.; Sen, D. DNA-enhanced peroxidase activity of a DNA aptamer-hemin complex. *Chem. Biol.* **1998**, *5*, 505-517.

20. Zhang, R.; Wu, J.; Ao, H.; Fu, J.; Qiao, B.; Wu, Q.; Ju, H. A rolling circle-amplified G-quadruplex/hemin DNAzyme for chemiluminescence immunoassay of the SARS-CoV-2 protein. *Anal. Chem.* **2021**, *93*, 9933-9938.

21. Huang, W.; Huang, S. M.; Chen, G. S.; Ouyang, G. F. Biocatalytic metal-organic frameworks: promising materials for biosensing. ChemBioChem **2022**, e202100567.

22. Miao, P.; Gao, C.; Hao, M.; Zhang, C.; Li, Z.; Ge, S.; Song, Z.; Zhang, J.; Yan, M.; Yu, J. Ultrasensitive DNA detection based on inorganic-organic nanocomposite cosensitization and G-quadruplex/hemin catalysis for signal amplification. *ACS Appl. Mater. Interfaces* **2020**, *12*, 42604-42611.

23. Freeman, R.; Liu, X.; Willner, I. Chemiluminescent and chemiluminescence resonance energy transfer (CRET) detection of DNA, metal ions, and aptamer-substrate complexes using hemin/G-quadruplexes and CdSe/ZnS quantum dots. *J. Am. Chem. Soc.* **2011**, *133*, 11597-11604.

24. Ma, J.; Chen, G.; Bai, W.; Zheng, J. Amplified electrochemical hydrogen peroxide sensing based on Cu-porphyrin metal-organic framework nanofilm and G-quadruplex-hemin DNAzyme. *ACS Appl. Mater. Interfaces* **2020**, *12*, 58105-58112.

25. Zheng, J.; Wai, J. L.; Lake, R. J.; New, S. Y.; He, Z.; Lu, Y. DNAzyme sensor uses chemiluminescence resonance energy transfer for rapid, portable, and ratiometric detection of metal ions. *Anal. Chem.* **2021**, *93*, 10834-10840.

26. Chen, J.; Zhang, Y.; Cheng, M.; Mergny, J. L.; Lin, Q.; Zhou, J.; Ju, H. Highly active G-quadruplex/hemin DNAzyme for sensitive colorimetric determination of lead(II). *Microchim. Acta* **2019**, *186*, 786-794.

27. Stefan, L.; Denat, F.; Monchaud, D. Insights into how nucleotide supplements enhance the peroxidase-mimicking DNAzyme activity of the G-quadruplex/hemin system. *Nucleic Acids Res*. **2012**, *40*, 8759-8772.

28. Stefan, L.; Denat, F.; Monchaud, D. Deciphering the DNAzyme activity of multimeric quadruplexes: insights into their actual role in the telomerase activity evaluation assay. *J. Am. Chem. Soc.* **2011**, *133*, 20405-20415.

29. Wang, Z. G.; Wang, H.; Liu, Q.; Duan, F.; Shi, X.; Ding, B. Designed self-assembly of peptides with G-quadruplex/hemin DNAzyme into nanofibrils possessing enzyme-mimicking active sites and catalytic functions. *ACS Catal.* **2018**, *8*, 7016-7024.

30. Wang, J.; Cheng, M.; Chen, J.; Ju, H.; Monchaud, D.; Mergny, J. L.; Zhou, J. An oxidatively damaged G-quadruplex/hemin DNAzyme. *Chem. Commun.* **2020**, *56*, 1839-1842.

31. Wang, Z.; Zhao, J.; Bao, J.; Dai, Z. Construction of metal-ion-free G-quadruplex-hemin DNAzyme and its application in S1 nuclease detection. *ACS Appl. Mater. Interfaces* **2016**, *8*, 827-833.

32. Millange, F.; Serre, C.; Ferey, G. Synthesis, structure determination and properties of MIL-53as and MIL-53ht: the first Cr^{III} hybrid inorganic-organic microporous solids: $Cr^{III}(OH).(O_2C\text{-}C_6H_4\text{-}CO_2).(HO_2C\text{-}C_6H_4\text{-}CO_2H)_x$. *Chem. Commun.* **2002**, *8*, 822-823.

33. Zheng, F.; Guo, S.; Zeng, F.; Li, J.; Wu, S. Ratiometric fluorescent probe for alkaline phosphatase based on betaine-modified polyethylenimine via excimer/monomer conversion. *Anal. Chem.* **2014**, *86*, 9873-9879.

34. Pu, M.; Ma, Y.; Wan, J.; Wang, Y.; Wang, J.; Brusseau, M. L. Activation performance and mechanism of a novel heterogeneous persulfate catalyst: Metal organic framework MIL-53(Fe) with Fe(II)/Fe(III) mixed-valence coordinative unsaturated iron center. *Catal. Sci. Technol.* **2017**, *7*, 1129-1140.

35. Wang, S.; McGuirk, C. M.; Ross, M. B.; Wang, S.; Chen, P.; Xing, H.; Liu, Y.; Mirkin, C. A. General and direct method for preparing oligonucleotide-functionalized metal-organic framework nanoparticles. *J. Am. Chem. Soc.* **2017**, *139*, 9827-9830.

36. Chen, Y.; Qiu, D.; Zhang, X.; Liu, Y.; Cheng, M.; Lei, J.; Mergny, J. L.; Ju, H.; Zhou, J. Highly sensitive biosensing applications of a magnetically immobilizable covalent G-quadruplex-hemin DNAzyme catalytic system. *Anal. Chem.* **2022**, *94*, 2212-2219.

37. Kong, D. M.; Xu, J.; Shen, H. X. Positive fffects of ATP on G-quadruplex-hemin DNAzyme-mediated reactions. *Anal. Chem.* **2010**, *82*, 6148-6153.

38. Du, J. J.; Yuan, Y. P.; Sun, J. X.; Peng, F. M.; Jiang, X.; Qiu, L. G.; Xie, A. J.; Shen, Y. H.; Zhu, J. F. New photocatalysts based on MIL-53 metal-organic frameworks for the decolorization of methylene blue dye. *J. Hazard. Mater.* **2011**, *190*, 945-951.

39. Yoon, J. W.; Seo, Y. K.; Hwang, Y. K.; Chang, J. S.; Leclerc, H.; Wuttke, S.; Bazin, P.; Vimont, A.; Daturi, M.; Bloch, E.; Llewellyn, P. L.; Serre, C.; Horcajada, P.; Greneche, J. M.; Rodrigues, A. E.; Ferey, G. Controlled reducibility of a metal-organic framework with coordinatively unsaturated sites for preferential gas sorption. *Angew. Chem. Int. Ed.* **2010**, *49*, 5949-5952.
40. Liu, Q.; Zeng, C.; Ai, L.; Hao, Z.; Jiang, J. Boosting visible light photoreactivity of photoactive metal-organic framework: Designed plasmonic Z-scheme Ag/AgCl@MIL-53-Fe. *Appl. Catal., B* **2018**, *224*, 38-45.
41. Li, Y.; Chen, B.; Duan, X.; Chen, S.; Liu, D.; Zang, K.; Si, R.; Lou, F.; Wang, X.; Rønning, M.; Song, L.; Luo, J.; Chen, D. Atomically dispersed Fe-N-P-C complex electrocatalysts for superior oxygen reduction. *Appl. Catal., B* **2019**, *249*, 306-315.
42. Chen, H.; Liu, Y.; Cai, T.; Dong, W.; Tang, L.; Xia, X.; Wang, L.; Li, T. Boosting photocatalytic performance in mixed-valence MIL-53(Fe) by changing Fe(II)/Fe(III) ratio. *ACS Appl. Mater. Interfaces* **2019**, *11*, 28791-28800.
43. Chen, J.; Zhang, Y.; Cheng, M.; Guo, Y.; Šponer, J.; Monchaud, D.; Mergny, J. L.; Ju, H.; Zhou, J. How proximal nucleobases regulate the catalytic activity of G-quadruplex/hemin DNAzymes. *ACS Catal.* **2018**, *8*, 11352-11361.
44. Zhang, P.; Ouyang, Y.; Willner, I. Multiplexed and amplified chemiluminescence resonance energy transfer (CRET) detection of genes and microRNAs using dye-loaded hemin/G-quadruplex-modified UiO-66 metal-organic framework nanoparticles. *Chem. Sci.* **2021**,12, 4810-4818.
45. Mi, L.; Sun, Y.; Shi, L.; Li, T. Hemin-bridged MOF interface with double amplification of G-quadruplex payload and DNAzyme catalysis: ultrasensitive lasting chemiluminescence microRNA imaging. *ACS Appl. Mater. Interfaces* **2020**, 12, 7879-7887.
46. Chen, X. F.; Zang, H.; Wang, X.; Cheng, J. G.; Zhao, R. S.; Cheng, C. G.; Lu, X. Q. Metal-organic framework MIL-53(Al) as a solid-phase microextraction adsorbent for the determination of 16 polycyclic aromatic hydrocarbons in water samples by gas chromatography-tandem mass spectrometry. *Analyst* **2012**, *137*, 5411-5419.
47. Stadlbauer, P.; Islam, B.; Otyepka, M.; Chen, J.; Monchaud, D.; Zhou, J.; Mergny, J. L.; Sponer, J. Insights into G-quadruplex-hemin dynamics using atomistic simulations: implications for reactivity and folding. *J. Chem. Theory Comput.* **2021**, *17*, 1883-1899.
48. Shi, W.; Zhang, X.; He, S.; Huang, Y. $CoFe_2O_4$ magnetic nanoparticles as a peroxidase mimic mediated chemiluminescence for hydrogen peroxide and glucose. *Chem. Commun.* **2011**, *47*, 10785-10787.
49. Wasil, M.; Halliwell, B.; Grootveld, M.; Moorhouse, C. P.; Hutchison, D. C. S.; Baum, H. The specificity of thiourea, dimethylthiourea and dimethyl sulphoxide as scavengers of hydroxyl radicals. *Biochem. J.* **1987**, *243*, 867-870.
50. Monteagudo, J. M.; Durán, A.; San Martin, I.; Carnicer, A. Roles of different intermediate active species in the mineralization reactions of phenolic pollutants under a UV-A/C photo-Fenton process. *Appl. Catal., B* **2011**, *106*, 242-249.
51. Bancirova, M. Sodium azide as a specific quencher of singlet oxygen during chemiluminescent detection by luminol and cypridina luciferin analogues. *Luminescence* **2011**, *26*, 685-688.
52. Gallati, V. Peroxidase aus meerrettich: kinetische studien sowie optimierung der Aktivitätsbestimmung mit den Substraten H_2O_2 und 2,2'-Azino-di-(3-ethyl-benzthiazolinsulfonsäure-(6)) (ABTS). *J. Clin. Chem. Clin. Biochem.* **1979**, *17*, 1-7.
53. Chen, Q.; Li, S.; Liu, Y.; Zhang, X.; Tang, Y.; Chai, H.; Huang, Y. Size-controllable Fe-N/C single-atom nanozyme with exceptional oxidase-like activity for sensitive detection of alkaline phosphatase. *Sens. Actuators, B* **2020**, *305*, 127511-127520.
54. Arnao, M. B.; Cano, A.; Hernández-Ruiz, J.; GarcíBa-Cánovas, F.; Acosta, M. Inhibition by L-ascorbic acid and other antioxidants of the 2,2'-Azino-bis(3-ethylbenzthiazoline-6-sulfonic Acid) oxidation catalyzed by peroxidase: A new approach for determining total antioxidant status of foods. *Anal. Biochem.* **1996**, *236*, 255–261.

For Table of Contents Only